RSC Advances

PAPER

View Article Online
View Journal | View Issue

Cite this: *RSC Adv.*, 2017, **7**, 1075

Color tunable emission and energy transfer in $LaSi_3N_5:Ce^{3+},Tb^{3+}$ phosphors for UV white LEDs†

Fu Du, Weidong Zhuang,* Ronghui Liu,* Yuanhong Liu, Jiyou Zhong, Pin Gao, Xia Zhang, Wei Gao and Lengleng Shao

Received 28th October 2016
Accepted 29th November 2016

DOI: 10.1039/c6ra25915d

www.rsc.org/advances

A series of new blue-green emitting $LaSi_3N_5:Ce^{3+},Tb^{3+}$ phosphors were obtained through a high temperature solid-state method. The crystal structure, photoluminescence properties and energy transfer from Ce^{3+} to Tb^{3+} were investigated. The doped ions Ce^{3+} and Tb^{3+} were confirmed to occupy the same crystallographic sites as La^{3+} using a Rietveld structure refinement method. The emission spectra of these phosphors was composed of a blue emission band attributed to the d–f transition of Ce^{3+}, together with several sharp lines ascribed to the emission of Tb^{3+} under UV light excitation. Thus a color tunable emission from blue to green was obtained *via* controlling the doping concentration of Tb^{3+}. In addition, the mechanism of energy transfer, efficiency of energy transfer, chromaticity coordinates and thermal stability of these phosphors were investigated. The results indicated that the Ce^{3+},Tb^{3+} co-activated $LaSi_3N_5$ phosphors with color-tunable blue-green emission and high quantum efficiency may have potential for UV white LEDs.

1. Introduction

Phosphor-converted white light-emitting diodes (WLEDs) have received considerable attention as a new-fashioned lighting source due to their high conversion efficiency, long lifetime and environment-friendly characteristics compared with the conventional incandescent and fluorescent lamps.[1–3] Most commercially available WLEDs are fabricated by combining the yellow-emitting $Y_3Al_5O_{12}:Ce^{3+}$ phosphor with (In,Ga)N-LED chips.[4] However, the major shortcoming of this phosphor is the lack of a red spectral component, which results in a low color rendering index ($R_a < 75$) and high color temperature ($T_c > 7000$ K) limiting their application.[5] To further improve the luminescence efficiency of these LEDs, near-UV (380–420 nm, short as n-UV) LED chips combined with blue, green and red phosphors was reported.[6,7] Especially, w-LEDs fabricated with n-UV chips coated with tricolor (red, green and blue) phosphors are regarded as the main trend in the market of the LED lighting industry.[8,9] Therefore, it is essential to develop new phosphors that emit blue, green or red light, which can be efficiently excited by the n-UV LED chips.

Recently, Ce^{3+} doped $LaSi_3N_5$-based phosphors with blue emission have drawn much attention due to their intense emission and high thermal stability.[10] The structure of $LaSi_3N_5$, which was first reported by Inoue *et al.*[11] in 1980, is composed of a three-dimensional network with vertex-sharing $[SiN_4]$ tetrahedral. Moreover, $LaSi_3N_5$ are reported to hold similar structure of Si_3N_4, hinting that $LaSi_3N_5$ may have rigid skeleton structure and some other special properties. Thus, $LaSi_3N_5$ might be an interesting host for phosphor. In recent years, the luminescence properties of Ce^{3+}-activated $LaSi_3N_5$ blue phosphors have been studied.[10,12–14] In 2011, Park *et al.*[15] reported that both the excitation and emission bands were getting slightly shift to long wavelength by doping Al. It is well known that Ce^{3+} ions not merely exhibit excellent luminescent properties with broadband emission but also can act as an efficient sensitizer due to its high efficiency of energy transfer. Typically, the energy transfer from Ce^{3+} to Tb^{3+} has been widely studied and the energy could be transferred from the ^5D level of Ce^{3+} to the $^5D_{3,4}$ level of Tb^{3+} in the proper matrix.[16–19] Therefore, it is may be attractive to develop a new phosphor in $LaSi_3N_5$ matrix by Ce^{3+} and Tb^{3+} co-doping. To the best of our knowledge, the luminescence properties of $LaSi_3N_5:Ce^{3+},Tb^{3+}$, as well as the mechanism of energy transfer, have not been reported in the literature.

In this work, we have synthesized a series of $LSN:Ce^{3+},Tb^{3+}$ phosphors and studied the structure, photoluminescence properties, energy transfer mechanism and energy transfer efficiency in detail. The luminescent properties study suggests that $LSN:Ce^{3+},Tb^{3+}$ may have potential application for UV WLEDs.

2. Experimental

2.1 Synthesis

A series of Ce^{3+} and Ce^{3+},Tb^{3+}-activated $LaSi_3N_5$ (LSN) phosphors were prepared *via* conventional high temperature solid

National Engineering Research Center for Rare Earth Materials, General Research Institute for Nonferrous Metals, Grirem Advanced Materials Co., Ltd., Beijing 100088, PR China. E-mail: wdzhuang@126.com; griremlrh@126.com

† Electronic supplementary information (ESI) available: XRD patterns of $La_{1-x}Si_3N_5:xCe^{3+}$ and $La_{1-y}Si_3N_5:yCe^{3+}$; ET models for Ce^{3+}–Tb^{3+} in the $LaSi_3N_5$ host. See DOI: 10.1039/c6ra25915d

state reactions. The raw materials LaN (99.5%), CeN (99.5%), and TbN (99.99%) were supplied by General Research Institute for Nonferrous Metals, and Grirem Advanced Materials Co. Ltd, Beijing, China, together with Si_3N_4 (>99.9%) bought from Sigma-Aldrich. The starting powders were weighted and mixed in an agate mortar for 15 min per each sample. All these operation were performed in a purified-nitrogen-filled glove box with oxygen and water vapor content maintained below 1 ppm. The mixed powders were placed in BN crucible and heated at 1900 °C for 10 h with pressure of nitrogen gas maintained at 2.0 MPa in the graphite resistance furnace. The prepared phosphors were cooled down to room temperature followed by ball-milling and water washing.

2.2 Characterization

The phase purity of samples was examined by the X-ray diffraction (XRD, Rigaku, Japan) with Co-Kα radiation (λ = 0.178752 nm), performing at 40 kV and 100 mA in the 2θ range from 10° to 80° with scanning speed of 6° per minute. The data for Rietveld structure refinement were collected from D8 Focus diffractometer (Bruker) operating at 40 kV and 40 mA with Cu Kα radiation (λ = 1.54 Å). The morphology of $LaSi_3N_5$:0.09-Ce^{3+},0.08Tb^{3+} was inspected by using scanning electron microscopy (SEM, S4800, Hitachi, Japan). Diffuse reflection spectra were measured on a UV-vis-NIR spectrophotometer (Shimadzu UV-2550) attached to an integral sphere and using $BaSO_4$ as reference standard. The photoluminescence (PL) and photoluminescence excitation (PLE) spectra were measured on a Hitachi F-4500 spectrophotometer equipped with a 150 W Xe lamp as the excitation source. The decay curves of Ce^{3+} with different Tb^{3+} concentrations were measured by a TemPro-01 time-resolved fluorescence spectrophotometer (Horiba Jobin Yvon, Japan) with a tunable pulse laser radiation as the excitation source. The Commission International de L'Eclairage (CIE) chromaticity coordinates were obtained from a HAAS-2000 light (Everfine, China). All above measurements were performed at room temperature.

3. Results and discussion

3.1 Crystal structure and morphology

Fig. 1(a) depicts the powder XRD patterns of the as-prepared LSN:0.09Ce^{3+}, LSN:0.08Tb^{3+}, LSN:0.09Ce^{3+},0.08Tb^{3+} phosphors. All the diffraction peaks of these samples are consistent with the JCPDS Standard Card No. 86-1858 of $CeSi_3N_5$, suggesting phase purities were formed and with the space group $P2_12_12_1$. The peaks were shown no obvious shift due to the very close ion radii of La^{3+} (1.06 Å), Ce^{3+} (1.03 Å) and Tb^{3+} (0.923 Å). Here, $CeSi_3N_5$ were chosen as references and reasons are following: first, the nitridosilicates $LnSi_3N_5$ (Ln = Ce, Pr, Nd) compounds are isostructural with $LaSi_3N_5$ as reported by Michael *et al.* It is worth noting that the lattice parameters of *a*, *b*, *c* and *V* for $LaSi_3N_5$ and $CeSi_3N_5$ are basically same;[20] second, the phase purity of $LaSi_3N_5$ are obtained by Zhou,[21] Ibrahim[12] and Suehiro,[10] and all of the diffraction peaks of $LaSi_3N_5$ accompanying with different doping rare earth Ce^{3+} are in good

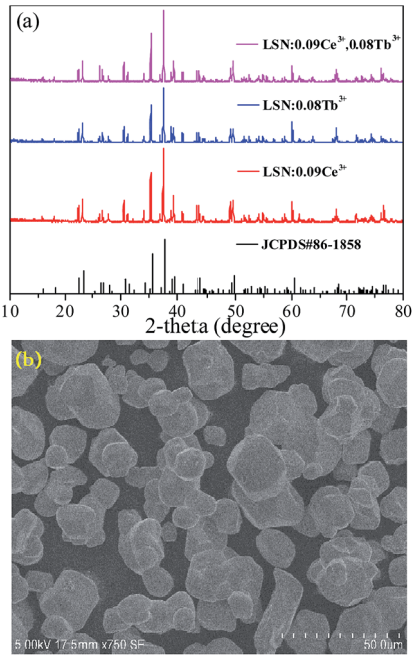

Fig. 1 (a) Powder XRD patterns of $La_{0.91}Si_3N_5$:0.09Ce^{3+}, $La_{0.92}Si_3N_5$:0.08Tb^{3+} and $La_{0.83}Si_3N_5$:0.09Ce^{3+},0.08Tb^{3+} phosphors. The standard data of $CeSi_3N_5$ (JCPDS No. 86-1858) is show as a reference. (b) SEM image of the as-prepared $La_{0.83}Si_3N_5$:0.09Ce^{3+},0.08Tb^{3+} phosphor.

agreement with $CeSi_3N_5$. However, few peaks in the 2θ range at 47–52°are observed in the samples prepared by Park *et al.*[14,15] and they are regarded as impurity peaks compared with the JCPDS 42-1144 of $LaSi_3N_5$. It is possible that the JCPDS standard pattern of $LaSi_3N_5$ should be further confirmed. To further confirm the structure of the obtained samples, Rietveld structure refinement of $LaSi_3N_5$ has been performed by using the Fullprof suite software,[22] as shown in Fig. 2. The crystal structure data of LSN (reported by Woike[23]) is used as the initial structure model and the main cell parameters and residual factors are summarized in Table 1. All of the peaks are obtained with goodness of fit parameters R_{wp} = 11.3, R_p = 8.82, R_{exp} = 7.33 and χ^2 = 2.37, indicating that all atom positions, residual

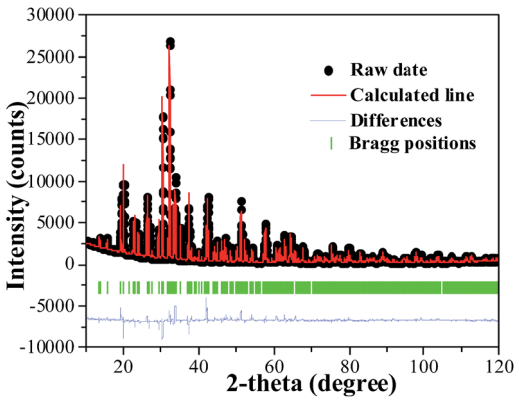

Fig. 2 Rietveld refinement of the XRD pattern of $LaSi_3N_5$. Bragg reflections are indicated with green tick marks.

Table 1 Selected crystallographic parameters from Rietveld refinement for the $LaSi_3N_5$ sample

Formula	$LaSi_3N_5$
X-ray source	Cu Kα
2θ (deg)	10–120
Symmetry	Orthorhombic
Space group	$P2_12_12_1$
Lattice parameters	$a = 7.85$ Å, $b = 11.26$ Å, $c = 4.81$ Å $\alpha = \beta = \gamma = 90^\circ$
Residual factors	$R_p = 8.82\%$, $R_{wp} = 11.3\%$, $R_{exp} = 7.33$, $\chi^2 = 2.37$

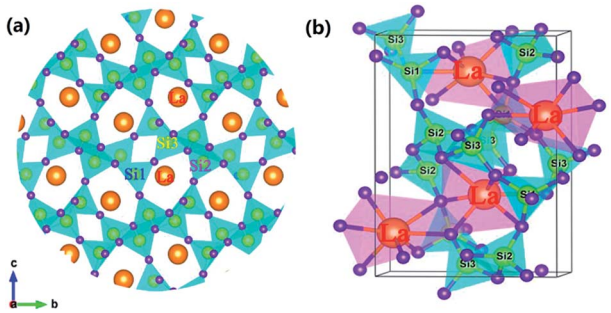

Fig. 3 (a) Crystal structure of $LaSi_3N_5$ along *a*-axis direction. The orange, yellow and purple represent the La, Si and N atoms, respectively. (b) The same coordination environment of La atoms.

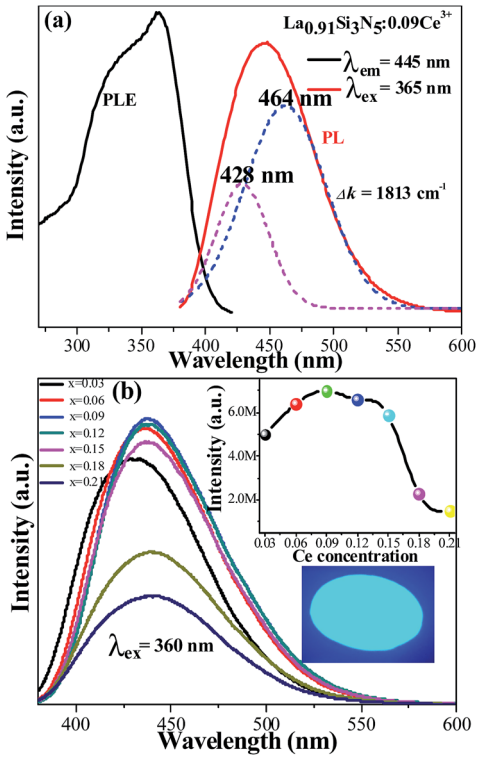

Fig. 4 (a) PL and PLE spectra of the as-synthesized LSN:0.09Ce^{3+} phosphor; (b) the emission spectra of LSN:xCe^{3+} with different Ce^{3+} contents. The inset above shows PL intensity of the LSN:Ce^{3+} samples as a function of the Ce^{3+} concentration and the inset below shows the photograph of the LSN:0.09Ce^{3+} phosphor under 365 nm excitation.

factors and temperature factors well suitable the reflection condition. Fig. 3(a) and (b) represent the crystal structure of LSN. In the LSN host, there is only one La site and La atom is located between the corresponding pentagonal holes which occur at one unit intervals along the *c*-axis, indicating that there is only one kind of crystallographic site for Ce^{3+} ion in this phosphor. The fundamental of LSN consists of SiN_4 tetrahedra that are linked by sharing their corners to form rings of five tetrahedral units. The characteristics of LSN structure are similar to Si_3N_4, which means that LSN may have intrinsically the same properties as silicon nitride, such as thermally stability. The morphology of $LaSi_3N_5$:0.09Ce^{3+},0.08Tb^{3+} sample was obtained by SEM shown in Fig. 1(b). Most particles show nearly spherical with clear edges and average diameter of about 15 μm, which is sufficiently separated from other particles. It is revealed that the particles may be suitable for fabricating with whites LEDs. Therefore, it is indicate that the synthesis conditions are appropriate.

3.2 Luminescence properties of Ce^{3+},Tb^{3+} doped and co-doped $LaSi_3N_5$ phosphors

Fig. 4(a) shows the PLE and PL spectra of the LSN:0.09Ce^{3+} phosphor. The sample shows an excitation band from 250 to 425 nm, indicating that it is suitable for the excitation absorption of the n-UV LED chip. At the excitation of 360 nm, the phosphor exhibits an asymmetric emission spectrum that covers the region from 375 to 540 nm with a peak centered at 445 nm. The doublet bands attributed to the Ce^{3+} ions from the 5d excited state to the $^2F_{5/2}$ and $^2F_{7/2}$ ground states cannot be distinguished directly. Furthermore, the emission spectra can be fitted into two well-separated Gaussian components (the dotted lines) with peak at 428 nm (23 364 cm^{-1}) and 464 nm (21 551 cm^{-1}). The energy gap between two bands is calculated to be 1813 cm^{-1}, which is very closed to the theoretical value of ~2000 cm^{-1}.[24,25] This result illustrates that Ce^{3+} ions substitute only one site in host lattice. Fig. 4(b) shows the intensity of PL spectra of LSN:xCe^{3+} with different doping Ce^{3+} contents (x = 0.03, 0.06, 0.09, 0.12, 0.15, 0.18, 0.21). The peak wavelength shows a red-shifting from 425 nm to 446 nm, which can be explained by the increased energy transfer between the 5d energy levels[26,27] and the enhanced crystal-field strength with the increasing Ce^{3+} content. The optimal emission intensity is obtained around 0.09 due to the concentration quenching effect (inset in Fig. 4(b)). The critical energy transfer distance (R_c) can be calculated using the following relation:[28]

$$R_c = 2\left(\frac{3V}{4\pi x_c N}\right)^{1/3} \quad (1)$$

where V is the volume of the unit cell, x_c is the critical concentration, N is the number of cations in the unit cell that can be substituted by the activator ions. In this host, V = 423.342 $Å^3$, x_c = 0.09 and N = 4, the critical distance is calculated to be 13.1 Å.

The PLE and PL spectra of LSN:0.09Ce^{3+} (a), LSN:0.08Tb^{3+} (b) and LSN:0.09Ce^{3+},0.08Tb^{3+} (c) are presented in Fig. 5. It can be

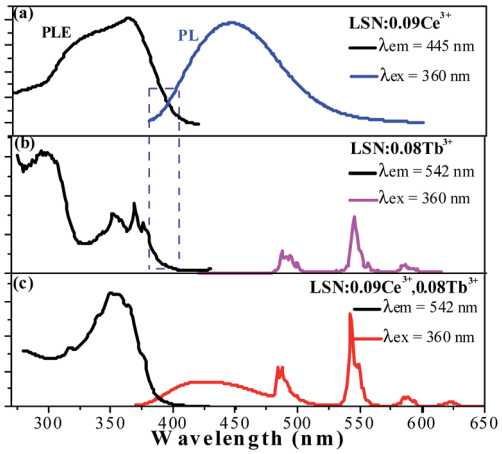

Fig. 5 The PL and PLE spectra of the as-synthesized LSN:0.09Ce^{3+} phosphor (a), LSN:0.08Tb^{3+} (b), and LSN:0.09Ce^{3+},0.08Tb^{3+} (c).

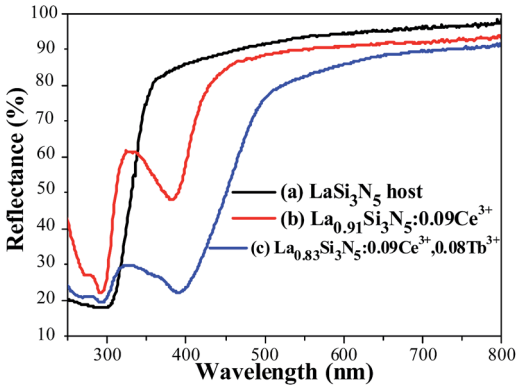

Fig. 6 Reflectance spectra of $LaSi_3N_5$ host (a), $La_{0.91}Si_3N_5$:0.09Ce^{3+} (b), and $La_{0.83}Si_3N_5$:0.09Ce^{3+},0.08Tb^{3+} (c).

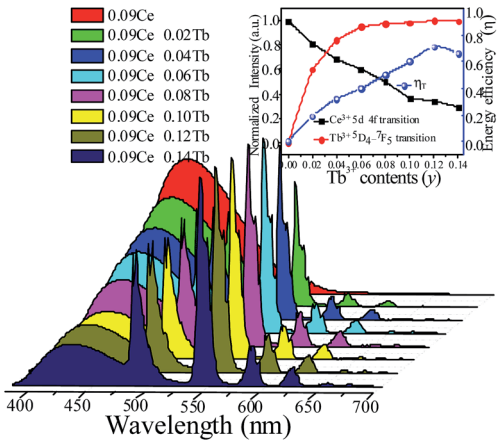

Fig. 7 PL spectra for LSN:0.09Ce^{3+},yTb^{3+} phosphors on Tb^{3+} doping content (*y*) excited at 360 nm. The inset shows the emission intensity of Ce^{3+} and Tb^{3+} with different Tb^{3+} contents and energy transfer efficiency on changing Tb^{3+} contents.

seen that excitation bands of Tb^{3+} are observed in the region from 300 to 450 nm, which could be referred to the f–f transition absorption of the Tb^{3+} ions. Under 360 nm excitation, the PL spectra of LSN phosphor singly doped with Tb^{3+} shows several weak emissions with peaks at 485, 542, 582 and 623 nm, due to the typical $^5D_4 \rightarrow {}^7F_J$ ($J = 6, 5, 4, 3$) multiple transitions of the Tb^{3+} ions.[29] However, as a green phosphor, it is hard to be applied in LED due to the lack of efficiency. In order to enhance the absorption intensity in the n-UV region for the Tb^{3+} emission, Ce^{3+} ions can be co-doped as sensitizers to transfer excitation energy to Tb^{3+} ions. It is observed that there is significant spectral overlap between the emission band of LSN:0.09Ce^{3+} and the PLE spectrum of LSN:0.08Tb^{3+} from Fig. 5(a) and (b). Energy transfer is expected to occur from Ce^{3+} to Tb^{3+} in LSN host, it can be further confirmed in Fig. 5(c). At the excitation of 360 nm, the emission intensity of LSN:0.09Ce^{3+},0.08Tb^{3+} in the region from 375 to 485 nm decreases compared with LSN:0.09Ce^{3+}, while the green lines from Tb^{3+} simultaneously increases. To further investigate the energy absorption of the $LaSi_3N_5$ host lattice, the reflectance spectra of LSN, LSN:0.09Ce^{3+}, and LSN:0.09Ce^{3+}, 0.08Tb^{3+} phosphors are presented in Fig. 6. The $LaSi_3N_5$ host exhibits low energy absorption in the UV region, which is assigned as the host absorption. However, two obvious broad absorption bands with peaking at 298 nm and 380 nm of the LSN:0.09Ce^{3+} are observed due to the f–d absorption of the Ce^{3+} ions. Moreover, the absorption band of LSN:0.09Ce^{3+},0.08Tb^{3+} is similar to LSN:0.09Ce^{3+}. The PLE spectrum and reflectance spectrum demonstrate that LSN:Ce^{3+},Tb^{3+} has broad absorption bond, which matches well with n-UV LED chips.

In order to study the relative intensities of the two emissions, a series of LSN:0.09Ce^{3+},yTb^{3+} phosphors have been prepared. Fig. 7 shows the emission spectra of LSN:0.09Ce^{3+},yTb^{3+} phosphors with *y* varying from 0 to 0.14 excited at 360 nm. With the increase of Tb^{3+} concentration, it is directly observed that the PL intensity of the Ce^{3+} decreases monotonically, whereas the green emission peaks of Tb^{3+} reach a maximum value at $y = 0.12$, and then decrease due to the nonradiative energy transfer of Tb^{3+}. This result strongly illustrates the energy transfer from the Ce^{3+} to Tb^{3+} ions in the LSN host lattice and is shown in the inset of Fig. 7. Therefore, the CIE of the LSN:Ce^{3+},Tb^{3+} phosphor could be tuned by appropriately adjusting the relative ratio of Ce^{3+}/Tb^{3+}. The energy transfer efficiency (η_T) from the Ce^{3+} to Tb^{3+} can be calculated by the following equation:[30,31]

$$\eta_T = 1 - \frac{I_S}{I_{S0}} \quad (2)$$

where I_S and I_{S0} are the luminescence intensity of the sensitizer (Ce^{3+}) ion in the presence and absence of the activator (Tb^{3+}), respectively. The inset of Fig. 7 displays the curve of η_T of Ce^{3+}–Tb^{3+} in LSN:0.09Ce^{3+},yTb^{3+}. As Tb^{3+} content increases, the distance between Ce^{3+} ions and Tb^{3+} ions becomes shorter, which enhances the efficient energy transfer. The optimal η_T (~71%) is obtained when *y* reached 0.12.

3.3 Energy transfer mechanism of LSN:Ce^{3+},Tb^{3+} phosphors

In order to further verify the process of energy transfer from Ce^{3+} to Tb^{3+} in LSN:Ce^{3+},yTb^{3+}, the fluorescence decay curves of

Ce^{3+} were measured by monitoring at 430 nm with excitation of 360 nm. As shown in Fig. 8, the decay curve of LSN:Ce^{3+} is agreeable to the single exponential rule with a lifetime of about 38.26 ns, due to single luminescent center in the host. However, the rest of decay curves deviates from the single exponential function and this phenomenon becomes more obvious with increase concentration of the Tb^{3+}. Therefore, the experimental curves were fitted by the sum of two exponential decays using the formula:

$$I(t) = I_0 + A_1 \exp(-t/\tau_1) + A_2 \exp(-t/\tau_2) \quad (3)$$

where the $I(t)$ represents the luminescence intensity at time t, A_1 and A_2 are constants, τ_1 and τ_2 are the decay times for the exponential components. The average decay time (τ) were estimated to be 26.44, 25.37, 21.84, 17.43, 14.76, 13.06 and 12.98 ns with function for the LSN:Ce^{3+},yTb^{3+} phosphors with $y = 0.02$, 0.04, 0.06, 0.08, 0.10, 0.12 and 0.14, respectively. The lifetimes of the Ce^{3+} ions decreased, which is the direct evidence for energy transfer from Ce^{3+} to Tb^{3+}. Moreover, the energy transfer efficiency from Ce^{3+} to Tb^{3+} was also calculated from the decay lifetime by the equation:[19]

$$\eta_T = 1 - \frac{\tau_S}{\tau_{S0}} \quad (4)$$

where τ_S and τ_{S0} are the lifetimes of Ce^{3+} ions with and without the presence of Tb^{3+} ions, respectively. As shown in the inset of Fig. 8, the energy transfer efficiency gradually increased and reached 65.86% for Tb^{3+} concentrations at $y = 0.12$, which is closed to the above result (~71%).

Normally, the energy transfer from sensitizer to activator may take place *via* exchange interaction and electric multipolar interaction.[32,33] The exchange interaction would take place when the critical distance (R_c) between the doping ions was shorter than 4 Å. Base on the eqn (1), x_c is the total concentration of Ce^{3+} and Tb^{3+} ion. For LSN:0.09Ce^{3+},0.08Tb^{3+} sample, V = 423.342 Å^3, $x_c = 0.17$ and $N = 4$, thus the R_c is determined to be 10.6 Å. It can be inferred that there is no mechanism of exchange interaction because the value of R_c (10.6 Å) is larger

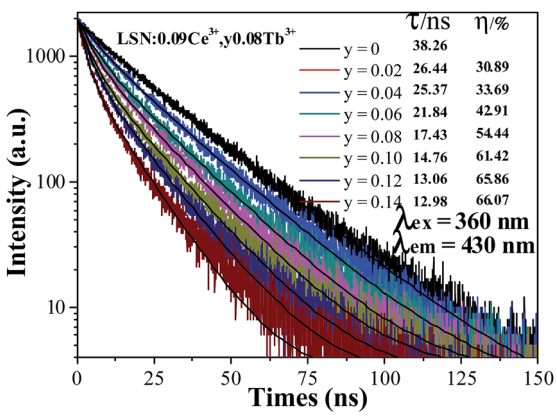

Fig. 8 Decay curves for the luminescence of Ce^{3+} ions in LSN:0.09Ce^{3+},yTb^{3+} phosphors (excited at 360 nm, monitored at 430 nm).

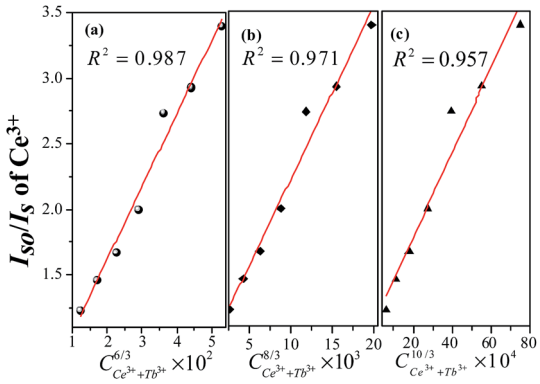

Fig. 9 Dependence of I_{S0}/I_S of Ce^{3+} on (a) $C^{6/3}$, (b) $C^{8/3}$ and (c) $C^{10/3}$. The red lines indicate the fitting behaviors.

than 4 Å. The energy transfer occurs *via* multipolar interaction based on the Dexter theory:[34]

$$\eta_0/\eta \propto C^{n/3} \quad (5)$$

where η_0 and η are the luminescence quantum efficiencies of the sensitizer (Ce^{3+}) ion in the absence and presence of the activator (Tb^{3+}), C is the sum concentration of Ce^{3+} and Tb^{3+}. The value of η_0/η can be approximately calculated by the I_{S0}/I_S (relative luminescence intensity ratio). The value of n is 6, 8, and 10 for dipole–dipole, dipole-quadrupole and quadrupole–quadrupole interactions, respectively. The relationships between I_{S0}/I_S and $C^{n/3}$ are illustrated in Fig. 9. It can be observed that the linear reaches the optimal when $n = 6$ with R^2 = 0.987, indicating that energy transfer from Ce^{3+} to Tb^{3+} in the $LaSi_3N_5$ host should mainly through the dipole–dipole interaction. The energy transfer model Ce^{3+}–Tb^{3+} in the $LaSi_3N_5$ is presented in Fig. S2.†

3.4 Thermal stability and chromaticity coordinates of LSN:Ce^{3+},Tb^{3+} phosphors

The thermal stability of phosphor is one of key parameters for practical phosphors. The temperature dependence of the luminescence for the LSN:0.09Ce^{3+},0.12Tb^{3+} phosphor under 360 nm excitation was investigated as a function of temperature in the range of 50–200 °C, as shown in Fig. 10. As the temperature is increased to 200 °C, the PL intensities of Ce^{3+} and Tb^{3+} decrease to 44% and 80% of the corresponding initial value (50 °C), which suggests that LSN:Ce^{3+},Tb^{3+} is a promising green phosphor for UV white LED. The shift of CIE coordinates is neglectable ($x = 0.2763$, $y = 0.4439 \rightarrow x = 0.2788$, $y = 0.4452$) due to the relative weak component of blue emission. As the essential of thermal quenching is the result of interaction between electron and lattice under varying temperatures, leading to nonradiative transitions. Since the d–f transition of Ce^{3+} is more affected by crystal field environment than f–f transition of Tb^{3+}, thus, the reason for different degradation rate of Ce^{3+} and Tb^{3+} is due to different degree of interactions between transition electron and lattice.

The CIE chromaticity diagram and a series of digital photographs of LSN:0.09Ce^{3+},yTb^{3+} phosphors upon 365 nm

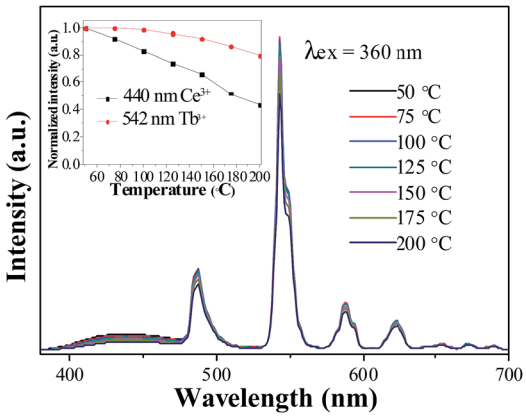

Fig. 10 Temperature-dependent emission spectra of LSN:0.09Ce^{3+},0.12Tb^{3+} phosphor. Inset shows the relative emission intensities as a function of temperature.

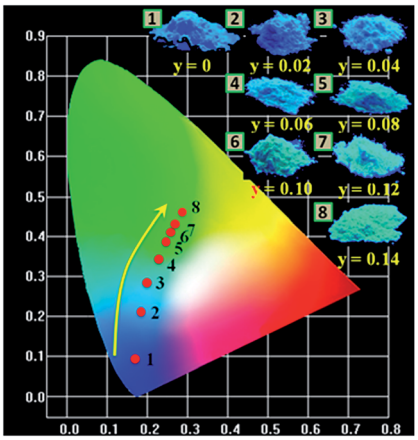

Fig. 11 CIE chromaticity coordinates diagram of LSN:0.09Ce^{3+},yTb^{3+} (y = 0, 0.02, 0.04, 0.06, 0.08, 0.10, 0.12, 0.14) (point no. 1-8) and the digital photographs of corresponding samples under 365 nm UV lamp.

UV lamp excitation are presented in Fig. 11. The values of CIE (x, y) for LSN:0.09Ce^{3+},yTb^{3+} with different doping contents are listed in Table 2. It can be found that color-tunable of LSN:0.09Ce^{3+},yTb^{3+} phosphors can be obtained with increasing content of Tb^{3+} due to efficient Ce^{3+}–Tb^{3+} energy transfer. The corresponding features of the chromaticity coordinates for the LSN:0.09Ce^{3+},yTb^{3+} phosphors could be changed from blue (0.1842, 0.0947) to green (0.2845, 0.4653) by adjusting the different emission compositions of the Ce^{3+} and Tb^{3+} concentration. Based on the results, it is clear that new blue-green emitting LSN:0.09Ce^{3+},yTb^{3+} phosphors can be efficiently excited in the UV range. It is suggesting that LSN:Ce^{3+},Tb^{3+} phosphor can act as a potential blue-green phosphor for WLEDs.

Table 2 CIE chromaticity coordinates (x, y) for LSN:0.09Ce^{3+},yTb^{3+} (y = 0, 0.02, 0.04, 0.06, 0.08, 0.10, 0.12, 0.14) phosphors upon excitation at 365 nm

Sample no.	Sample composition (y)	CIE coordinates (x, y)
1	0	(0.1824, 0.0947)
2	0.02	(0.1924, 0.2092)
3	0.04	(0.2216, 0.2899)
4	0.06	(0.2400, 0.3423)
5	0.08	(0.2553, 0.3853)
6	0.10	(0.2703, 0.4287)
7	0.12	(0.2763, 0.4439)
8	0.14	(0.2845, 0.4653)

4. Conclusions

A series of Ce^{3+}/Tb^{3+} co-activated $LaSi_3N_5$ phosphors were synthesized through high temperature solid state reaction. The obtained phosphors show a broad excitation spectral range from 280 to 400 nm, which can meet the application requirements for UV LED chips. The energy transfer from Ce^{3+} to Tb^{3+} in LSN host has been investigated by PL and PLE spectra, together with the contents of Tb^{3+}, and the decay curves of Ce^{3+}. The energy transfer from Ce^{3+} to Tb^{3+} was mainly *via* a dipole–dipole reaction. The critical distance of energy transfer was calculated and has also been evaluated by the concentration quenching method. By adjusting Tb^{3+} doping concentration in LSN:0.09Ce^{3+},yTb^{3+}, the emission of the phosphors can be tuned appropriately from blue (0.1824, 0.0947) to green (0.2845, 0.4653) and the luminescence efficiency of green emission reached the maxima at the Tb^{3+} concentration of 0.12. The $LaSi_3N_5$:Ce^{3+},Tb^{3+} phosphor could be potentially used as a green emitting phosphor for WLEDs.

Acknowledgements

The present work was supported by the Ministry of Science and National Key Research Program of China (No. 2016YFB0400600) and (No. 2016YFB0400605) and the National Key Basic Research Program of China (2014CB643801).

References

1 C. Feldmann, T. Justel, C. R. Ronda and P. J. Schmidt, *Adv. Funct. Mater.*, 2003, **13**, 511–516.
2 R. J. Xie, N. Hirosaki, T. Suehiro, F. F. Xu and M. Mitomo, *Chem. Mater.*, 2006, **18**, 5578–5583.
3 L. Chen, R. H. Liu, W. D. Zhuang, Y. H. Liu, Y. S. Hu, X. F. Zhou and X. L. Ma, *J. Alloys Compd.*, 2015, **627**, 218–221.
4 Y. C. Jia, Y. J. Huang, Y. H. Zheng, N. Guo, H. Qiao, Q. Zhao, W. Z. Lv and H. P. You, *J. Mater. Chem.*, 2012, **22**, 15146–15152.
5 X. Q. Piao, K. Machida, T. Horikawa, H. Hanzawa, Y. Shimomura and N. Kijima, *Chem. Mater.*, 2007, **19**, 4592–4599.
6 Z. G. Xia, J. Q. Zhuang, L. B. Liao, H. K. Liu, Y. Luo and P. Du, *J. Electrochem. Soc.*, 2011, **158**, 359–362.
7 C. H. Huang and T. M. Chen, *J. Phys. Chem. C*, 2011, **115**, 2349–2355.
8 J. Zhou, Z. G. Xia, M. X. Yang and K. Shen, *J. Mater. Chem.*, 2012, **22**, 21935–21941.

9 J. Y. Zhong, W. D. Zhuang, X. R. Xing, R. H. Liu, Y. F. Li, Y. H. Liu and R. S. Hu, *J. Phys. Chem. C*, 2015, **119**, 5562–5569.
10 T. Suehiro, N. Hirosaki, R. J. Xie and T. Sato, *Appl. Phys. Lett.*, 2009, **95**, 051903.
11 Z. Inoue, M. Mitomo and N. Ii, *J. Mater. Sci.*, 1980, **15**, 2915–2920.
12 I. Ibrahim, Z. Lences, L. Benco, M. Hrabalova and P. Sajgalik, *J. Eur. Ceram. Soc.*, 2014, **34**, 2705–2712.
13 A. Yaguchi, T. Suehiro, T. Stao and N. Hirosaki, *Appl. Phys. Express*, 2011, **4**, 022101.
14 L. Y. Cai, X. D. Wei, H. Li and Q. L. Liu, *J. Lumin.*, 2009, **129**, 165–168.
15 J. W. Park, S. P. Singh and K. S. Sohn, *J. Electrochem. Soc.*, 2011, **158**, 184–188.
16 J. S. Kim, P. E. Jeon, Y. H. Park, J. C. Choi, H. L. Park, G. C. Kim and T. W. Kim, *Appl. Phys. Lett.*, 2004, **85**, 3696.
17 X. G. Zhang and M. L. Gong, *Dalton Trans.*, 2014, 2465–2472.
18 D. L. Geng, M. M. Shang, Y. Zhang, H. Z. Lian and J. Lin, *Inorg. Chem.*, 2013, **52**, 13708–13718.
19 Z. G. Xia and R. S. Liu, *J. Phys. Chem. C*, 2012, **116**, 15604–15609.
20 M. Woike and W. Jeitschko, *Inorg. Chem.*, 1995, **34**, 5105–5108.
21 Y. Zhou, Y. Yoshizawa, K. Hirao, Z. Lences and P. Sajgalik, *J. Eur. Ceram. Soc.*, 2011, **31**, 151–157.
22 J. Rodriguez-Carvajal, *Curr. Pharm. Des.*, 2001, **26**, 12–19.
23 M. Woike and W. Jeitschko, *Z. Kristallogr.*, 1996, **211**, 813.
24 G. R. Hatfield, B. Li, W. B. Hammond, F. Reidinger and J. Yamanis, *J. Mater. Sci.*, 1990, **25**, 4032–4035.
25 N. Guo, Y. H. Song, H. P. You, G. Jia, M. Yang, K. Liu, Y. H. Zheng, Y. J. Huang and H. J. Zhang, *Eur. J. Inorg. Chem.*, 2010, **29**, 4636–4642.
26 J. L. Wu, G. Gundiah and A. K. Cheetham, *Chem. Phys. Lett.*, 2007, **441**, 250–254.
27 T. Suehiro, N. Hirosaki, R. J. Xie, K. Sakuma, M. Mitomo, M. Ibukiyama and S. Yamada, *Appl. Phys. Lett.*, 2008, **92**, 191904.
28 Y. L. Zheng, W. D. Zhuang, X. R. Xing, J. Y. Zhong, R. H. Liu and Y. S. Hu, *RSC Adv.*, 2016, **6**, 68852–68859.
29 M. M. Shang, G. G. Li, X. J. Kang, D. M. Yang, D. L. Geng and J. Lin, *ACS Appl. Mater. Interfaces*, 2011, **3**, 2738–3746.
30 G. Zhu, Y. H. Wang, Z. P. Ci, B. Liu, Y. R. Shi and S. Y. Xin, *J. Lumin.*, 2012, **132**, 531–536.
31 M. Shang, G. Li, D. Geng, D. Yang, X. Kang, Y. Zhang, H. Lian and J. Lin, *J. Phys. Chem. C*, 2012, **116**, 10222–10231.
32 F. Lahoz, I. Martin, R. J. Mendez and P. Nunez, *J. Chem. Phys.*, 2004, **120**, 6180–6190.
33 R. Reisfeld, E. Greenberg, R. Velapoldi and B. Barnett, *J. Chem. Phys.*, 1972, **56**, 1698.
34 D. L. Dexter, *J. Chem. Phys.*, 1953, **21**, 836–850.